# EVALUATION OF A RANGE IMAGING SENSOR CONCERNING RESOLUTION AND ILLUMINATION

J. A.S. Centeno [a] *, B. Jutzi [b]

[a] Geomatics Department, Federal University of Parana,
Po.Box 19001, 81.531-990 Curitiba, Paraná, Brazil - centeno@ufpr.br
[b] Institute of Photogrammetry and Remote Sensing, Karlsruhe Institute of Technology (KIT),
Kaiserstr. 12, 76128 Karlsruhe, Germany - boris.jutzi@kit.edu

**Commission I, WG I/2**

**KEY WORDS:** Intensity, resolution, accuracy, range imaging, RIM, close range.

**ABSTRACT:**

The introduction of range imaging devices opens new applications in the field of close range photogrammetry, especially for measuring as well as modeling of objects and internal environments. To evaluate the real potential of such devices, it becomes necessary to know its limitations and capabilities. Within this work aspects related to the range variation and accuracy (i) and resolution (ii) of a range imaging device (PMD CamCube 2.0) will be investigated. i) One drawback of the data which is captured with RIM sensors is the absolute range accuracy. Various studies have been proposed on this subject. Our study focuses especially on the tuneable shutter speed of the sensor. For high shutter speed strong variations on the measured range and intensity, due to the low signal-to-noise ratio (SNR) can be expected. For low shutter speed a systematic error on the range measurement, caused by sensor saturation effects and the measurement principle can be expected. ii) If areas in different ranges are partly illuminated a non-reliable range value is obtained, due to superimposed single measured range values within the instantaneous field of view (IFOV), which implies a combination of the surfaces at different ranges. The measured range depends on the illuminated area size and the distance between the surfaces. Having this in mind, a special reference object was constructed, a test box with various sized slots at its front. The idea for the experiment is to determine the smallest slot where the beam can penetrate without suffering the multiple surfaces effect at different ranges. The measured slot size provides a minimum area in a specific range to obtain reliable RIM measurements. Therefore an experimental setup was build up and the derived results are presented.

## 1. INTRODUCTION

The basic principle to unify advantages between active sensors and the simultaneous capturing of an image for an area of dynamical 3D applications in close range is recently given by range imaging (RIM) sensors. RIM sensors allow capturing a range image and a co-registered (active and passive) intensity image simultaneously with high repetition rate (up to 100 releases per second) in close range. The measured intensity strongly depends on the used wavelength (usually close infrared) of the illumination source and the surface characteristic. Various manufacturers provide RIM sensors, namely the Swiss Ranger (www.mesa-imaging.ch), the PMD Vision (www.pmdtec.com), and the O3D series (www.ifm.de).

In order to identify attractive applications for RIM sensors it is necessary to investigate the quality of the captured data. The requirements in terms of data quality depend on the purpose of the survey and are discussed in the literature, for example by Zhou et al. (2008) or Karel (2008). The optical characteristics of the camera and the emitted light, as also the environmental influences and the properties of the measured surface play an important role in this context. For the evaluation of the quality of surveys using this technology, these factors must be considered and is the motivation for this investigation.

## 2. RANGE & RESOLUTION

The RIM sensor provides a range image and a co-registered (active and passive) intensity image per single release. By utilizing a light source (diode array) the scene is illuminated and the backscattered light is captured by semiconductor detectors (CMOS array). The emitted energy, generally near infra-red light, propagates with the speed of light c. Depending on the distance the incoming light is temporal delayed by dt that can be measured at the sensor and enables to compute the distance between the camera and the surface:

$$R = c \cdot dt / 2. \quad (1)$$

The distance to the illuminated surface is computed by the phase dφ between the phase of the transmitted signal and the received signal (Möller et al., 2005). Due to the ambiguity characteristic of the phase a limited unique range imposes the practical limitations of the RIM sensors. From other sensor systems different techniques are known to solve this problem in order to obtain a unique range, e.g. by utilizing different modulation frequencies as most continuous-wave (CW) modulated laser scanner and radar systems do or by (pseudo) random modulation. The ambiguous range subject is close related to the phase unwrapping problem which is extensively discussed in the radar interferometry community. Further to overcome this problem Jutzi (2009) utilized the Goldstein 2D unwrapping procedure.

The time delay can be computed in terms of the modulation frequency $f_m$:

$$dt = d\varphi / (2 \cdot \pi \cdot f_m). \quad (2)$$

Substituting in Equation 1 the range R can be computed by the frequency and phase difference with

* Corresponding author: Jorge A.S. Centeno

$$R = (c \cdot d\varphi) / (4 \cdot \pi \cdot f_m). \quad (3)$$

Some systematic errors are expected for the measurements and can be predicted like, for example, the inhomogeneous scene illumination. The measured range is influenced by the total amount of incident light, e.g. depending on the Signal-to-noise-ratio (SNR) caused by the inhomogeneous scene illumination the measurement as well as different reflectivity of the illuminated surfaces result in more or less reliable measurements. This fact results from different physical effects of the RIM sensor, both the semiconductor detector and the camera electronics (Kolb et al., 2009). Obviously as it has to be expected the active illumination decreases from the centre, as depicted in Figure 1.

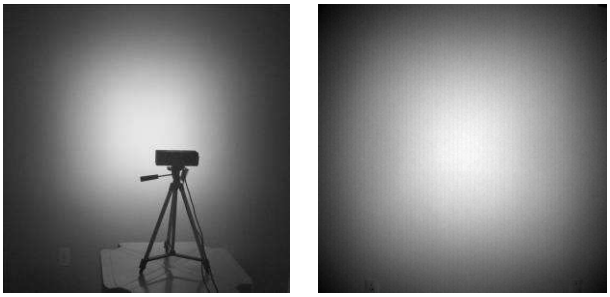

a b

Figure 1: Intensity distribution of a RIM sensor (PMD [Vision] CamCube 2.0) while illuminating a homogeneous and flat surface. a) captured with a external IR camera including RIM sensor in the front, b) measured with the RIM sensor itself.

According to Gokturk et al. (2004), the range resolution $R_R$ is determined by the number of divisions that the unambiguous range can be reliably divided (discretization) and is described by

$$R_R = C / (2 \cdot f_m) \cdot (A / P_{laser} \cdot q_e \cdot r \cdot T)^{1/2}. \quad (4)$$

where

$f_m$: modulation frequency,
$q_e$: quantum efficiency,
T: integration time,
$P_{laser}$: optical power of the light source,
r: reflectivity,
A: total illuminated area (target),
C: constant.

Equation 4 reveals that the range resolution can be improved by increasing the integration time. It has to be considered that a maximal value for sensor saturation is given. The range resolution can be improved by minimizing the illuminated area, which is a critical limitation of RIM sensors. The maximum image resolution is currently 204x204 Pixels.

In this work we present the results of two experiments aiming to establish the optimal configuration of a PMD sensor for close range surveying. Therefore, two aspects are investigated: i) the effects of the shutter speed of the sensor on the range variation and accuracy and ii) the capability of the sensor to measure within small areas. Therefore, the experiments are divided in two parts, as presented as follows.

## 3. EXPERIMENTS

This study focuses on the effects of the shutter speed of the sensor on the range variation and accuracy (3.1) and spatial resolution (3.2).

### 3.1 Shutter speed effects on the range measurement

For high shutter speed strong variations on the measured range and intensity, due to the low signal-to-noise ratio (SNR) and for low shutter speed a systematic error on the range measurement, caused by sensor saturation effects and the measurement principle can be expected. Therefore an experimental setup was built up and images of a reference target with various shutter speeds were captured. For the experiments a PMD [Vision] CamCube 2.0 was utilized to capture data of a flat surface (wall) as depicted in Figure 1.

Images from different distances to the wall and varying the integration time for each distance were captured and analyzed. The distance was varied stepwise with 108, 125, 172, 215, 260, and 310cm. For each distance, the integration time was varied between 500µs and 7000µs (Table 1).

| Integration time [µs] |
|---|
| 500 |
| 1000 |
| 1500 |
| 1700 |
| 1800 |
| 1900 |
| 2000 |
| 2500 |
| 3000 |
| 3500 |
| 4000 |
| 4500 |
| 5000 |
| 5300 |
| 5500 |
| 6000 |
| 7000 |

Table 1: Settings for the integration time.

The first step was to calibrate the camera in order to reduce the geometrical distortions introduced by the optical system. Camera calibration was performed using the method proposed by Zhang (2000) that is based on the recognition of edges of a rectangular chessboard in a series of images taken from different angles and directions. The results of the calibration are the focal length $c_{focal}$, the position of the principal point $(i_0,j_0)$, the skew coefficient and the image distortion coefficients (radial and tangential distortions).

In order to compute the position of the 3D point associated to each pixel the image was first geometrically corrected, using the parameters computed in the camera calibration step. After image rectification a rectangular central area of the image was extracted to perform the analysis. Each range measurement was converted to relative three-dimensional coordinates within this central area.

The angle of each range measurement is given by the position of the pixel and the internal orientation parameters of the optical system, according to the pin hole camera model (Khongsab,

2009). The horizontal and vertical angles must be carefully computed for each position in order to get the relative position of each point in the three-dimensional space using a polar coordinate system:

$$y = (i - i_0) \cdot pixel\_size,$$
$$x = (j - j_0) \cdot pixel\_size, \quad (5)$$

$$r^2 = x^2 + y^2, \quad (6)$$

$$Z = R \cdot \cos( \operatorname{atan}( r / c_{focal} ) ), \quad (7)$$

$$X = x \cdot Z / c_{focal}, \quad (8)$$

$$Y = y \cdot Z / c_{focal}. \quad (9)$$

Taking into account that the surface (wall) may not lie parallel to the sensor, the principal components transformation was applied to the point cloud. Because the variations along the Z axis are lower, the third eigenvalue is associated to the Z coordinate. For each integration time, the standard deviation of the Z component was the computed.

### 3.2 Resolution

The second aspect that is investigated within this work is related to the "*mixed pixel*" that appear if two surfaces in different ranges are within the instantaneous field of view (IFOV). To give an example for two surfaces in different ranges, two superimposed measurements of the range are derived, where one is closer and the other one is further away from the sensor. In practice for instance a small gap affects the measurement and non-reliable range values are derived, because the superimposed measurement is a combination of the different ranges depending on the illuminated area of each surface and the distance in between the surfaces.

If a sensor is used to capture data of objects with details, such as gaps or thin depressions (for instance marks on stones or sculptures) the expected range depends on the amount of the sensor distinguish both surfaces. Considering that a surface with thin gaps lies parallel to the sensor plane, three options are possible:

- the beam hits only the front surface
- the beam penetrates the slot and hits only the rear surface
- the beam hits the front and rear surface

In the last case the measured value is a combination of both superimposed measured range values.

The idea of this experiment is the same as proposed by Centeno et al. (2010) for terrestrial laser scanner (TLS), to determine the smallest slot where the beam can penetrate and return to the sensor without suffering the multiple surfaces effect of different ranges. The measured size provides a minimum area related to a specific range where reliable RIM measurements can be obtained.

For this purpose, a test box with a front panel consisting out of rectangular parallel slots with varying width and a closed rear panel was constructed (Figure 2). The widths of the slots are 1, 2, 3, 4, 5, 6, 7, 8, 9, 10, 15, 20 and 25mm. The depth from front to rear panel is about 255mm. The box was mounted parallel to the image plane and scanned from different distances.

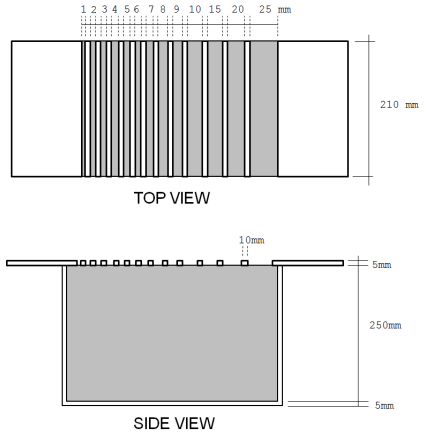


Figure 2: Sketch illustrating the widths of the slots and depth of the test box.

## 4. RESULTS

### 4.1 Shutter speed effects on the range measurement

Figure 3 shows the range variation by the standard deviation of the range measurements for a flat surface as a function of the integration time for different ranges: 108, 125, 172, 215, 260, and 310cm.

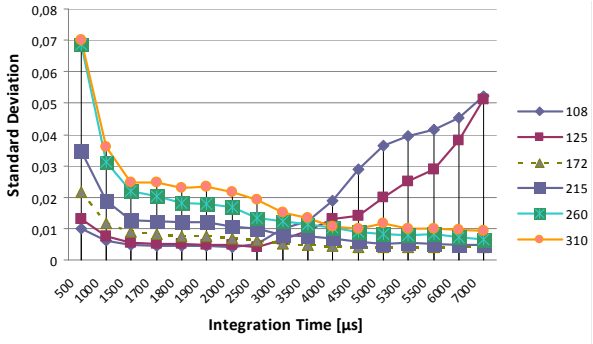


Figure 3: Standard deviation of the range for different integration times and distances.

The plots can be separated in two groups for the analysis:

i) For short ranges, distances of 108cm and 125cm, the standard deviation is low for lower integration times and grows as the integration time is increased due to saturation effects. It is also noticed that extreme small integration times also increase the standard deviation slightly.

ii) If the range is equal or larger than 172cm the standard deviation decreases with the integration time. For short ranges the standard deviation increases due to the low SNR. The lowest standard deviation is obtained for integration times above 4000µs.

In this example the lowest range variation is achieved for integration times between 2500µs and 4000µs.

To investigate the range accuracy the histogram of the range values for every integration time were analyzed. They are depicted in Figure 4 and 5. The data was collected at 172cm range, the histograms show almost a normal distribution and differ slightly to the expected mean. If the range is 108cm, the

behavior is different. The histogram shows a normal distribution only for low integration times with an erroneous and systematical range shortening shift of the mean. If the integration time is increased up to saturating the sensor, the histogram shows a slightly range extending shift of the mean.

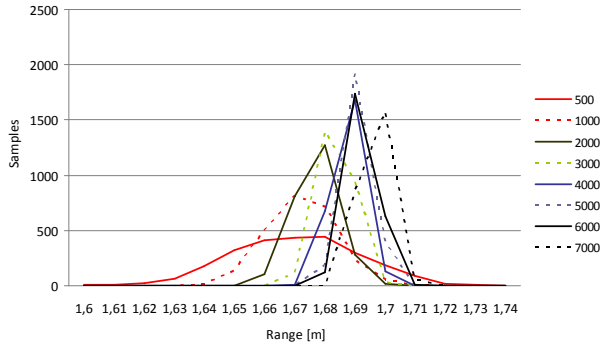


Figure 4: Histogram of the range for different integration times at 172cm range.

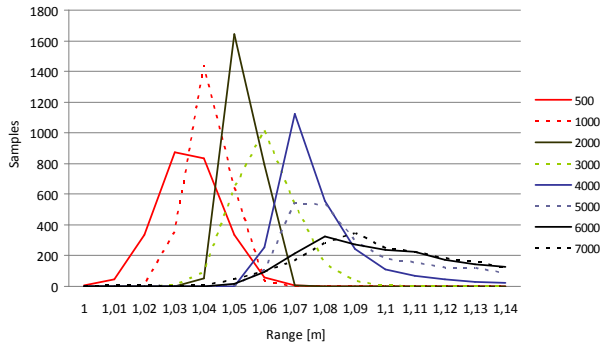


Figure 5: Histogram of the range for different integration times at 108cm range.

Figure 6 shows histograms of the measured data for the range 108cm and the integration times: t=2000µs, t=4000µs, and t=6000µs. It can be observed that the range values are more spread when the integration time is high. This might be caused by saturation effects by the measurement with the CMOS elements. Further it could be observed, that for an increasing integration time the measured range is more range extending (shift away from the sensor location).

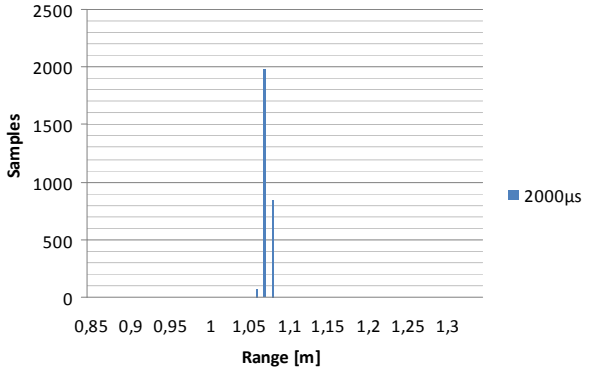


a

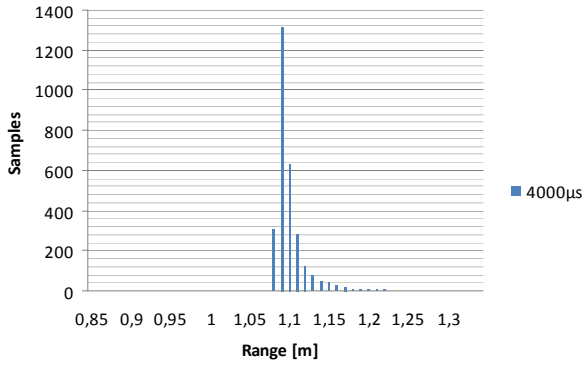


b

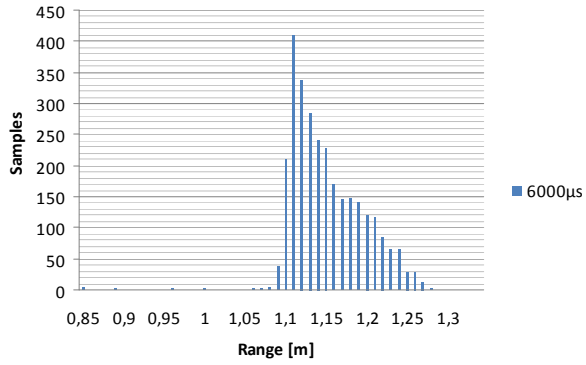


c

Figure 6: Histograms of the measured data for the range 108cm and various integration times. a) t=2000µs, t=4000µs, and t=6000µs.

The same spatial shift can be observed by each measured 3D point in Figure 7. The point cloud is more spread and noisy for higher integration times and the mean plane is shifted further from the sensor.

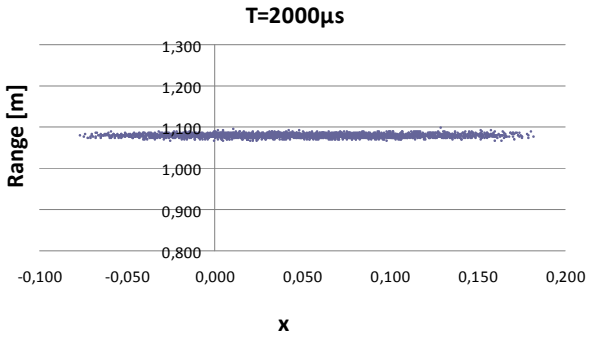


a

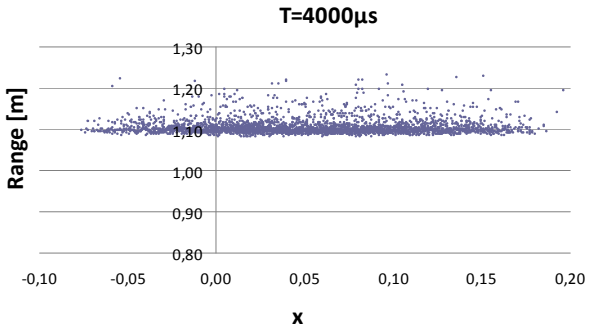


b

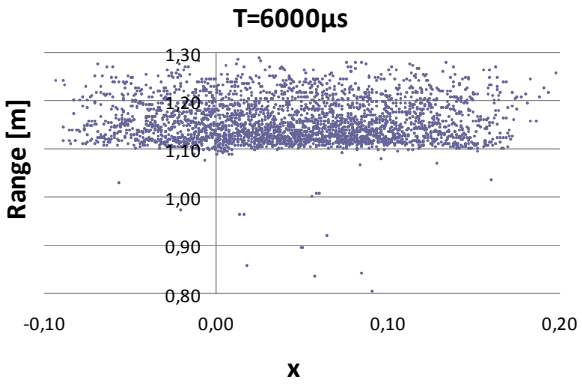


c

Figure 7: Examples of the point cloud shift and distribution for various integration times. a) 2000µs, b) 4000µs, and c) 6000µs.

### 4.2 Resolution

For the next experiment data of the test object, which is depicted in Figure 2, was captured. The captured data was transformed to Cartesian coordinates taking into account the interior orientation parameters of the sensor. Figure 8 shows the range distribution of the range data for the test box 140cm in front of the RIM sensor. Due to the visualization multiple measurement values can appear at the same location.

The front panel of the box is clearly visible at the range of 140cm, but the rear panel of the box appears as a curve, not flat. The depth of the test box is 25.5cm, therefore for reliable measurements 51cm will be expected due to the two ways, the way there and back of the light at the slots of the box. But it can be observed that for a large number of measurements greater than 165.5cm are given.

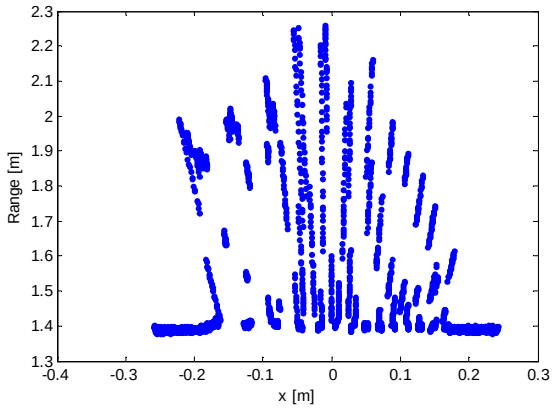


a

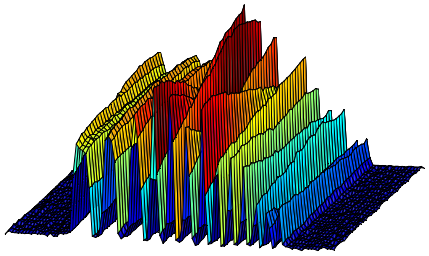

b

Figure 8: Measured data of the test object. a) range distribution, b) 3D visualization.

The wider slots, like the one that appears at the left side in Figure 8, may be affected by the reflection at the walls of the box, but this cannot be an explanation at the centre of the box, where the highest ranges are visible. A possible explanation is the occurrence of multiple reflections between the bottom and the frontal panel, although this was not experimentally verified. Figure 8b shows a 3D visualization of the derived range measurements. Obviously the slots were not exactly parallel, therefore the measured ranges along the borders of the slots shows some variation.

Figure 9 shows a histogram of the measured range values of the test box. The front panel is clearly visible by the highest peak at a range of about 140 cm. Again for the rear panel of the box a peak at 165.5cm would be expected. This peak does not appear. Instead, small peaks are noticed at ranges of about 188cm and 196cm, which is close to the range which would be derived by multipath reflection with 190.5cm, calculated by 140cm + 25.5cm + 25cm. Due to the oblique view on the rear panel of the test box, which can be seen on the plot in Figure 8a, the spreaded range distribution can be explained at this range. The largest range values are measured at ranges of about 225cm. In general these overestimated range values can only be explained by multipath effects. It is surprising that these effects exceed multiple times of the box depth.

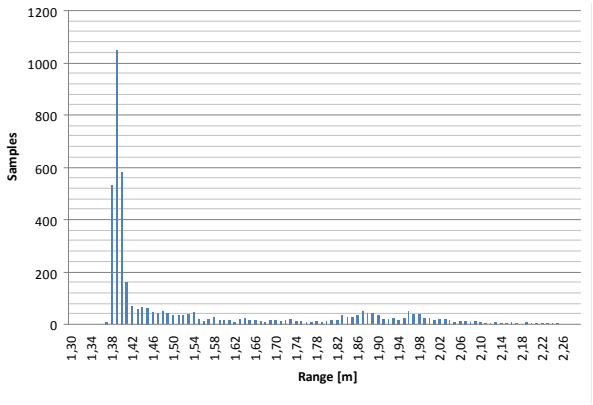


Figure 9: Histogram of the measured range for the test box.

As mentioned above for edges within the instantaneous field of view (IFOV) mixed range values are measured. Due to the slot size the measured range values are expected in between the range of the front and rear panel. If the range values are only affected at the borders of the slots and reliable measurements of the rear panel at the centre of the slots are derived the slot size can be seen as a measure for the spatial resolution of the RIM sensor. With other words for the thinnest slot where a range measurement from the rear panel could be derived the spatial resolution is determined for this specific range. The spatial resolution was measured for the test box in different ranges: 80, 110, 140, 210, 260, and 310cm. It was not possible to measure the resolution for greater distances, because a box with larger slots would be necessary and was not available.

Figure 10 shows the comparison between the measured values and the reference values derived by Equation 4, where the calibrated focal length has to be considered. In order to obtain a more realistic comparison, the computed values were truncated, because the test object allows only to measure integer values in mm. The data is very similar and follow the same linear trend.

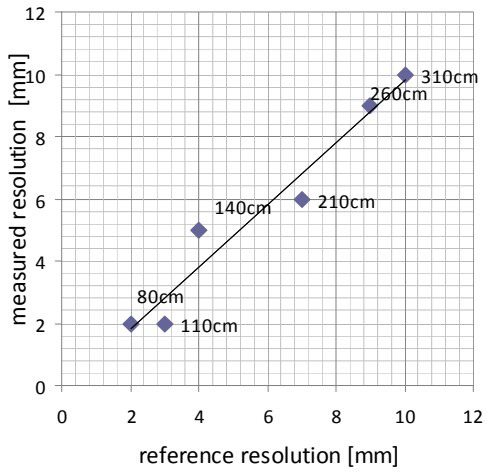


Figure 10: Comparison between the reference and the measured resolution.

Three aspects could be observed for the experiment:

i) The measured value is influenced by the presence of more than one surface within the IFOV. This is visible at pixels where the borders of the slot are presented. In this case, mixed pixel measurements are produced and the obtained range is a weighted average of the observed range of the multiple surfaces.

ii) The minimal gap that the camera is able to record depends on the range and is proportional to the reference resolution of the system. The experiment is suitable to estimate the spatial resolution of range images.

iii) The not predictable multiple path effects could be observed, which results in range measurements above the depth of the test box.

Considering Equation 4, the spatial resolution has practical limitations imposed by the illumination time and illuminated area on the surface. The integration time cannot be increased without the risk of introducing errors caused by sensor saturation. On the other hand, a better spatial resolution can be achieved reducing the illuminated area, which is only possible reducing the distance between the sensor and the object. The experiments show that there is a tradeoff between the range and the integration time. If the illuminated area is reduced to increase the resolution, then the integration time has to be reduced too.

## 5. CONCLUSIONS

The study shows some limitations of RIM devices by utilizing the PMD [Vision] CamCube 2.0. The low spatial resolution, which is expected to be improved in the coming years, limits the potential of such cameras when spatial detail is desired. It could be shown that the optimal accuracy is achieved by choosing an adequate integration time. It could also seen that when the illumination is too low, the camera produces noisy points that lie far from the camera, while when the integration time is too high the errors appear closer to the sensor.

The use of a test object to verify the spatial resolution of the RIM sensor could successfully shown. A remarkable and not predictable effect with the multipath reflection was noticed.

For future work the same study should be repeated for other imaging devices. The results can help to obtain the optimal integration time for different ranges and to predict problems when dealing with surfaces with relief details.

## ACKNOWLEDGEMENTS

This study has been made possible through the generous cooperation between the Karlsruhe Institute of Technology - KIT (Institute of Photogrammetry and Remote Sensing) and the Federal University Parana (Departamento de Geomatica).

## REFERENCES

Centeno, J. A.S., Vögtle, T., Wutke, J.D., Mitishita, E.A., 2010. Two Methods to Estimate the Spot Size of Terrestrial Laser Scanners. Journal of Surveying Engineering. doi:10.1061/(ASCE)SU.1943-5428.0000021.

Gokturk, S.B., Yalcin, H., Bamji, C., 2004. A Time-of-Flight Depth Sensor - System Description, Issues, and Solutions, IEEE Computer Society Conference on Computer Vision and Pattern Recognition Workshop, pp. 35–45, doi:10.1109/CVPR.2004.17.

Karel, W., 2008. Integrated range camera calibration using image sequences from hand-held operation. The International Archives of the Photogrammetry, Remote Sensing and Spatial Information Sciences 37 (Part B5).

Kolb, A., Barth, E., Koch, R., Larsen, L., 2009. Time-of-Flight Sensors in Computer Graphics. EUROGRAPHICS 2009/ M. Pauly and G. Greiner STAR – State of The Art Report.

Khongsab, P., 2009. Signal processing and performance evaluation of a PMD camera for space docking. Master Thesis. University essay from Luleå tekniska universitet/Space Science, Kiruna.

Jutzi, B., 2009. Investigations on ambiguity unwrapping of range images. In: Bretar, F., Pierrot-Deseilligny, M., Vosselman, G., (Eds) Laserscanning 2009. International Archives of Photogrammetry and Remote Sensing 38 (Part 3/W8), pp. 265-270.

Möller, T., Kraft, H., Frey, J., Albrecht, M., Lange, R., 2005. Robust 3D Measurement with PMD Sensors. In: Proceedings of the 1st Range Imaging Research Day at ETH Zurich, Zurich, Switzerland.

Zhang, Z., 2000. A flexible new technique for camera calibration, IEEE Transactions on Pattern Analysis and Machine Intelligence 22 (11), pp. 1330-1334.

Zhou, K., Zhao X., Zhou, J., Wang, F., Hu, S., 2008. Application of terrestrial laser scanning for heritage conservation in Yungang Grotto. The International Archives of the Photogrammetry, Remote Sensing and Spatial Information Sciences 37 (Part B5).